Since January 2020 Elsevier has created a COVID-19 resource centre with free information in English and Mandarin on the novel coronavirus COVID-19. The COVID-19 resource centre is hosted on Elsevier Connect, the company's public news and information website.

Socio-Economic Planning Sciences 83 (2022) 101228

Contents lists available at ScienceDirect

Socio-Economic Planning Sciences

journal homepage: www.elsevier.com/locate/seps

COVID-19 lockdowns and air quality: Evidence from grey spatiotemporal forecasts

Mingyun Gao [a,b,1], Honglin Yang [a,1], Qinzi Xiao [a,c,*], Mark Goh [b]

[a] School of Business Administration, Hunan University, Changsha, Hunan, 410082, PR China
[b] NUS Business School and The Logistics Institute-Asia Pacific, National University of Singapore, S(117592), Singapore
[c] Asper School of Business, University of Manitoba, Winnipeg, MB, R3T 2N2, Canada

ARTICLE INFO

Keywords:
PM2.5 forecasting
Spillover effect
Momentum effect
Grey spatiotemporal model

ABSTRACT

This paper proposes a novel grey spatiotemporal model and quantitatively analyzes the spillover and momentum effects of the COVID-19 lockdown policy on the concentration of PM2.5 (particulate matter of diameter less than 2.5 μm) in Wuhan during the COVID-19 pandemic lockdown from 23 January to 8 April 2020 inclusive, and the post-pandemic period from 9 April 2020 to 17 October 2020 inclusive. The results suggest that the stringent lockdowns lead to a reduction in PM2.5 emissions arising from a momentum effect (9.57–18.67%) and a spillover effect (7.07–27.60%).

1. Introduction

Strict lockdown policies to restrict movement control and to enforce working from home in order to combat the COVID-19 pandemic has helped major industrial centres in Asia such as Wuhan to return to economic normalcy. Consider the series of lockdown policies from 23 January to 8 April 2020 enforced on Wuhan and other cities in Hubei, China to curb the outbreak of COVID-19. This strict lockdown policy imposed on the Wuhan Metropolitan Area (WMA) involved suspending factory production, movement control, and working from home was an unprecedented move, albeit at massive economic and social costs [1]. Nevertheless, it was effective in controlling the outbreak [2], resulting in a spillover effect on reducing CO_2 emissions [3], household food management and waste [4], economic slowdown [5], and lowering the amount of PM2.5 emissions [6]. Such environmental improvements have also saved more lives. Chen et al. estimated that the reduction in PM2.5 emissions during the economic lockdown avoided a total of 3214 PM2.5 related deaths in China [7].

As the pandemic provides a context to observe and assess socio-economic changes nationally and regionally, we can study the effects of draconian lockdown policies on environmental improvement, namely the spillover and momentum effects. Doing so, we can then address the research question: are lockdown policies a blessing in disguise for heavily industrialized centres such as the WMA?

1.1. Motivation

The spillover effect is an eternality [8], stemming from an unpredicted or unrelated event of a socio-economic system. Correspondingly, the momentum effect stems from within a system, in that it is an empirically observed phenomena whereby events which have been trending in a certain direction for some time would be expected to continue to do so [9], akin to the momentum generated under a physical system. The momentum effect of a system can be traced through historical data [10], or through prediction modeling [11].

Air pollution would persist in its track unless intervened by the external system. In this case, the prediction of a PM2.5 concentration trend is possible, and the future state of air quality (labeled $PM2.5_{\text{Future Value}}$) can be approximated using the simulated prediction value (labeled $PM2.5_{\text{Simulated Prediction}}$) based on existing data (such as historical air quality and meteorological data [12]). The simulated predicted value comprises a current value ($PM2.5_{\text{Current Value}}$) and the momentum effect, namely,

$$PM2.5_{\text{Simulated Prediction}} = PM2.5_{\text{Current Value}} + \text{Momentum effect}.$$

When the intervention of external events (such as the pandemic) cannot be ignored, $PM2.5_{\text{Simulated Prediction}}$ cannot be a good predictor of $PM2.5_{\text{Future Value}}$ unless we consider the spillover effect caused by socioeconomic triggers such as plant closures and travel bans during a

* Corresponding author. School of Business Administration, Hunan University, Changsha, Hunan, 410082, PR China.
E-mail address: qzxiao97@hnu.edu.cn (Q. Xiao).
[1] Mingyun Gao and Honglin Yang contributed equally to this manuscript.

https://doi.org/10.1016/j.seps.2022.101228
Received 9 December 2020; Received in revised form 9 December 2021; Accepted 7 January 2022
Available online 11 January 2022

lockdown, namely,

$$PM2.5_{\text{Future Value}} = PM2.5_{\text{Simulated Prediction}} + \text{Spillover effect.}$$

Hence, the spillover effect can be measured through the simulated prediction and future value, since the future value is known in the next period.

Since the outbreak of COVID-19, several studies have been undertaken to discuss the spillover effect of a lockdown on air quality. For instance, Li and Tartarini [13] quantified the effect of the lockdown measures on outdoor air pollution levels in Singapore. Studying the spatiotemporal impact of COVID-19, Liu et al. noted that the lockdown reduced the overall amount of air pollutants in California [14], and found that the mitigation policies reduced the overall trend of NO_2 emissions in most target countries [15]. Assessing the level of PM2.5 from the 50 most polluted capital cities globally, Rodríguez-Urrego [16] found that cities under quarantine decreased PM2.5 by 12.5% on average, when comparing the air pollutants before and during COVID-19. Perera et al. modeled the potential future health benefits to children and adults, and reported that the air quality in New York continued to improve during the COVID-19 lockdown [17]. Such spillover effects of the lockdown policies are measured through the comparative analysis of the air pollutants during COVID-19 and those before the pandemic. Similarly, many cities in China are now in a post-pandemic period, with economic life returning to normalcy. The latest trade report announced that China had witnessed an 18.3% increase quarterly y-o-y in GDP performance in Q1 of 2021, the best result since 1993 [18]. For instance, in China's industrial heartland, Wuhan is a rapidly industrializing city, and is constantly shifting her urban planning, infrastructure, and industrial structure. Thus, the momentum effect of such socio-economic adjustments (such as the relocation of heavy industries, the construction of infrastructural facilities, and landscaping for the Military World Games) cannot be ignored in PM2.5 emissions. As the momentum effect is a component of $PM2.5_{\text{Simulated Prediction}}$, the prediction of PM2.5 concentration is therefore key to measuring the momentum and the spillover effects.

1.2. Literature review

The traditional air quality prediction methods focus on statistical or econometric models, which are based on economic or geographical phenomenon (such as seasonality, periodicity or spatiotemporal patterns [19]). Table 1 lists these representative methods.

As these statistical methods lack the ability to process a large amount of multidimensional [36], high-frequency and nonlinear data, Machine Learning, Artificial Intelligence [37] or Deep Learning (DL) [38] methods have been popular in PM2.5 forecasting. The latter methods usually provide better solutions to problems with high-dimension issues and nonlinearity, and they have shown to be more efficient in processing large datasets as a time series problem.

A high prediction precision of the DL methods can be achieved provided there are sufficient air quality indicators or high-frequency meteorological data [39], such as hourly or daily data. As research advances, environmental modelers find that the complex air pollution datasets can be decomposed into various frequency components [40,41]. Although successful in predicting the high-frequency components, both statistical econometrics and machine learning are not ideal for making projections particularly for systems with low-frequency components. Besides, with respect to the air quality indicators, there exist sparsity and uncertainty for two reasons. First, air quality is affected by factors such as pressure, temperature, humidity, and rainfall [42]. These factors will interact to produce physical and chemical reactions, rendering the analysis of air quality more dynamic, variable, and complex. Second, comprehensive air quality indicators are only available post 2014 for most cities in China, leaving research with barely sufficient annual and quarterly observations [43]. Under such situations of limited training data of the quality indicators, researchers have called on grey models, given their advantages of relatively easy computation and reliable model fitting [44].

Using the accumulative generating operator [45] and grey difference information principle [46], the grey model can mitigate data uncertainty and avoid the complex derivation of the data distribution [47]. However, the existing grey prediction models are usually used on time series data. Almost no consideration has been given to the spatial correlation of air pollution. From the literature, air quality evolution often exhibits regularity in time and space [48]. Particulate matter has high cyclicality and is easily affected by space [49], stagnating or diffusing to pollute the surrounding environment [50].

Therefore, this study seeks to apply a Spatio-Temporal Grey Model (STGM) to forecast PM2.5 emissions and to estimate the momentum and spillover effects. Compared to the grey models that are constructed based on a simple time series, the proposed model combines spatial

Table 1
Contemporary methods for forecasting air quality.

Source	Model	Study focus	City/region
Statistical econometric method			
Zhang et al.(2018) [20]	ARIMA	Monthly PM2.5 concentration	Fuzhou, China
Wang et al. (2017) [21]	GARCH	PM2.5 concentration	Shenzhen, China
Lei et al. (2019) [22]	Multiple regression	Daily average PM2.5, PM10, NO_2, and O_3 concentration	Macao
Samal et al. (2019) [23]	Combined SARIMA and Prophet model	RSPM, SO_2, NO_2, SPM	Bhubaneswar City, India
Machine learning/Artificial Intelligence/Deep Learning			
Sun & Sun (2017) [24]	Least squares support vector machines	Daily PM2.5 concentration	Baoding, China
García Nieto et al. (2018) [25]	Multilayer perceptron neural networks	Monthly average concentration of PM10	Oviedo region in Spain
Murillo-Escobar et al. (2019) [26]	Optimized support vector regression	Pollutant concentration including NO, NO_2, O_3, PM10, and PM2.5	Aburrá Valley, Colombia
Feng et al. (2019) [27]	Back propagation neural network	Daily pollutant emissions from open burnings	South China
Bai et al. (2019) [28]	LSTM	Hourly PM2.5 concentration	Beijing
Wen et al. (2019) [29]	Convolutional LSTM extended model	Hourly PM2.5 concentration	China
Bai et al. (2019) [30]	Stacked auto-encoders model	Hourly PM2.5 concentration	Three monitoring stations in Beijing
Zhang et al. (2020) [31]	Auto-encoder and bidirectional LSTM	Hourly PM2.5 concentration	Beijing
Grey model (GM)			
Chen & Pai. (2015) [32]	GM (1,1) model	Hourly inhalable particles	Taichung, Taiwan
Xiong et al. (2019) [33]	GM (1,1) model	Monthly air quality index	Shanghai
Xiong et al. (2020) [34]	MGM(1,2)	Fog and haze	Nanjing, China
Wu et al. (2019) [35]	Seasonal fractional-order grey model	Quarterly concentrations of PM2.5, PM10, NO_2, and CO_2	Xingtai and Handan

correlation with temporal correlation in the space-time series of particulate matter emissions.

1.3. Contributions

This paper makes several contributions, namely:

(i) this paper combines the GM(1,1) model with the spatial autoregressive model to propose a new STGM for PM2.5 trend forecasting.
(ii) this paper uses historical PM2.5 data to quantify the momentum effect on PM2.5 emissions during a lockdown.
(iii) this paper estimates the spillover effect of lockdown policies by comparing the forecast of PM2.5 with actual values.
(iv) the momentum effect of lockdown policies are estimated post-pandemic using the combined STGM-LSTM forecasting model.

The rest of the paper is organized as follows. Section 2 explores the framework of time series decomposition and Spatiotemporal Grey Models (STGM) to forecast the space-time PM2.5 series. The STGM is validated in Section 3 using the space-time datasets. Section 4 discusses the results. Section 5 concludes and offers some research directions.

2. Materials and method

The dataset of PM2.5 concentrations in this study is described in Section 2.1. Using STL (Seasonal and Trend decomposition using Loess), our study extracts three components, seasonal, monthly and daily, from the PM2.5 space-time series in Section 2.2. Then, this paper discussed the combined method of STGM and the LSTM network model to forecast PM2.5. For the trend forecasting, Section 2.3 provides STGM, which combines the classical GM(1,1) and spatial autoregressive models. For the daily component forecasting, Section 2.4 forms an LSTM network model. The combined PM2.5 forecasting model is summarized in Section 2.5.

2.1. Dataset

The Wuhan Metropolitan Area (WMA), also known as the Wuhan "1 + 8" city cluster, is a 100-km wide locale with Wuhan as the core and eight neighboring cities of Huangshi, Ezhou, Xiaogan, Huanggang, Xianning, Xiantao, Qianjiang, and Tianmen as satellites. To stem the spread of COVID-19, a series of lockdowns began on January 23, 2020 in WMA. As a result, there has been a marked improvement in the air quality in Wuhan [51]. To measure the spillover effect on environmental improvement during a lockdown, this study has therefore chosen WMA as the study area when constructing the PM2.5 forecasting model.

WMA has 26 air pollution monitoring stations (plotted as green bubbles), as shown in Fig. 1. The hourly concentrations of PM2.5 are recorded and published by the China National Environmental Monitoring Centre (http://www.cnemc.cn/sssj/). The station coordinates (such as latitude and longitude) are recorded, to construct the spatial weights matrix. We used the mean of the PM2.5 concentration from 0:00 to 23:00 h to represent the daily PM2.5 concentration [52], and we filled the missing data using multiple imputation, a common statistical process of replacing missing data with substituted values.

The dataset has three periods:(i) pre-pandemic (1 Jan. 2015 to 22 Jan. 2020), which was used to train and test the PM2.5 forecasting model; (ii) lockdown (23 Jan. to 8 April 2020), which was used to quantize the spillover effect of the lockdown; and (iii) post-pandemic (9 April to 17 Oct. 2020), which was used to quantize the momentum effect of the lockdown.

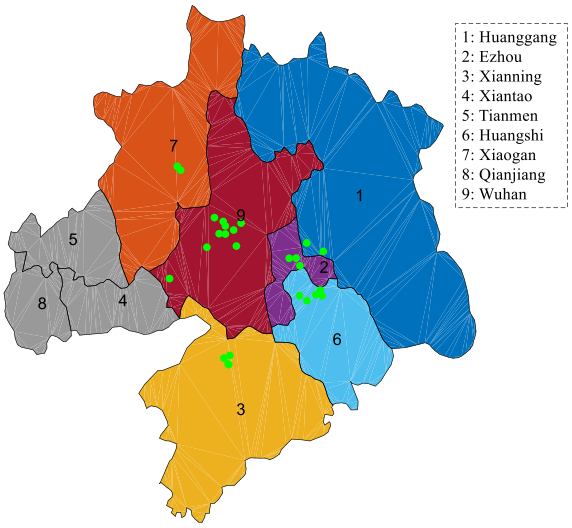

Fig. 1. Location of air quality stations in WMA.

2.2. Time series decomposition

The space-time series of PM2.5 data exhibits various cycles: daily, monthly or yearly. For each spatial unit in the series, it is often helpful to decompose the time series into components, each representing an underlying characteristic. For instance, the seasonal characteristic of the PM2.5 time series in a year has been mentioned in existing studies [53,54], namely, the concentration of PM2.5 during winter is higher than in summer. Further, there is a trend in PM2.5 data [55,56], which reflects the pollution over a longer time horizon.

Suppose the PM2.5 value of day d in month k for spatial unit i is $y_{i,k,d}$. Then, this value can be regarded as the sum of three components as shown in Equation (1)

$$y_{i,k,d} = s_i(k) + x_i^{(0)}(k) + e_{i,k,d} \tag{1}$$

where $s_i(k)$ is the seasonal component, which is the data fluctuation that recurs over a period of time. $x_i^{(0)}(k)$ is the trend component, which is the long term direction of the PM2.5 time-series data of spatial unit i. The trend component in PM2.5 data reflects the monthly weather pollution. The term $e_{i,k,d}$ denotes the remainder component.

Using the time series seasonal decomposition by STL [57], the monthly series is then fitted iteratively until the seasonal and trend components stabilize, and at the end of the process, the seasonal component $s_i(k)$ and trend component $x_i^{(0)}(k)$ are extracted from the original data series $y_{i,k,d}$, and the remainder component $e_{i,k,d}$ is found via Equation (2)

$$e_{i,k,d} = y_{i,k,d} - s_i(k) - x_i^{(0)}(k) \tag{2}$$

Fig. 2 shows the plots of the components. In the bottom left of Fig. 2, all of the seasonal components reveal a regular pattern. Clearly, the PM2.5 data possess periodicity by year; namely, the value in summer (June to September) is lower than that in winter (December to February). In the literature, the PM2.5 concentration decreases during

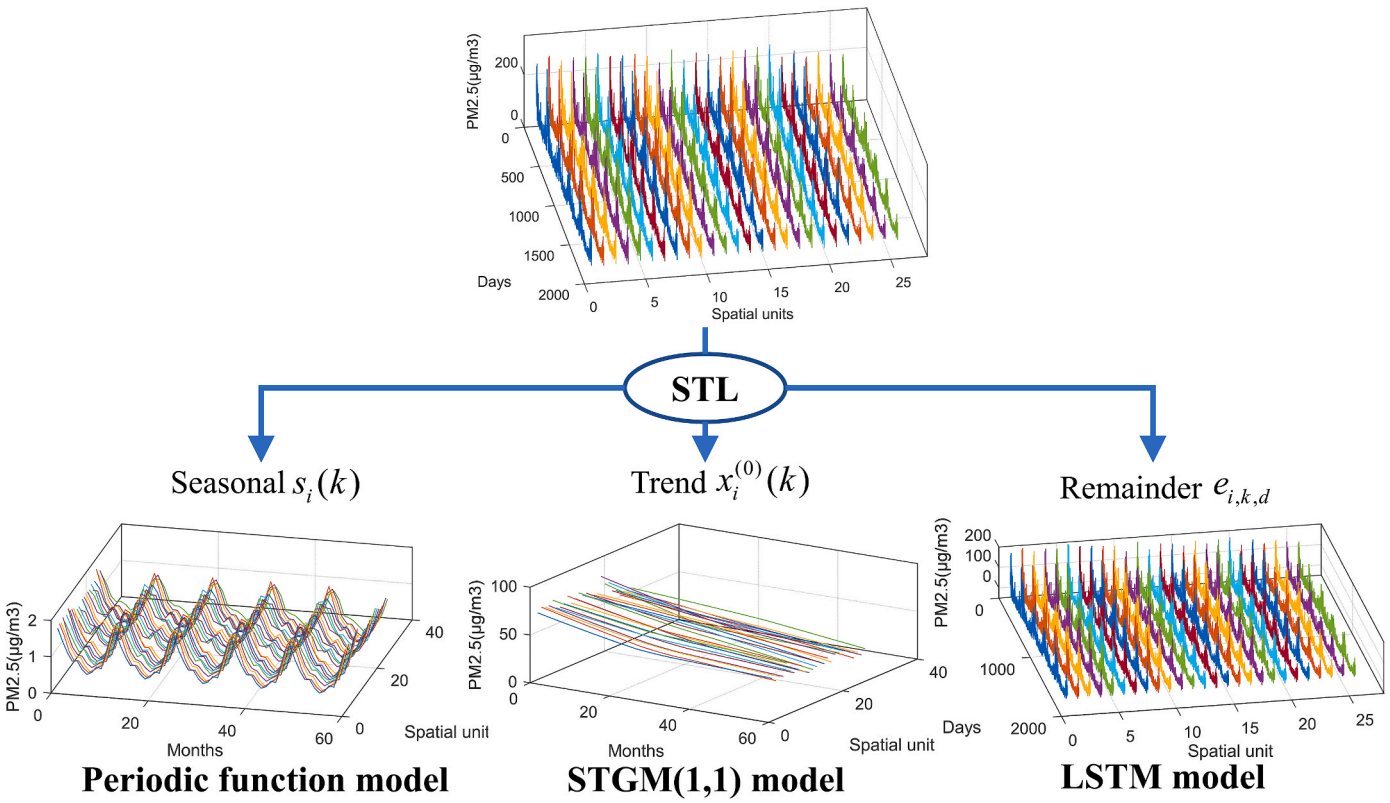

Fig. 2. Decomposition of PM2.5 space-time series.

the days with rain or wind [58]. Thus, this periodic phenomenon agrees with Wuhan's temperate continental climate, with most rainfall and windy in summer. The periodicity of the seasonal components is a year. Thus, these seasonal components can be set as a group of discrete periodic functions.

From the bottom centre of Fig. 2, all of the curves of the monthly trend components are monotone decreasing in time. Each curve appears to be exponential, which can be modeled using the classical GM(1,1). Considering the spatial structure of these observation stations, Moran's I test is then performed as shown in Fig. 3 (the full results are available as supplementary material).

From Fig. 3, all of the Moran's I in the 60 months exceeded the critical value ($I_0 = 0.04$), and the p-values are less than 0.01 (as $\lg(p)$ are below -2), namely, there is significant spatial dependence within these components for each month. Thus, spatial correlation cannot be ignored when developing the forecasting model for these trends.

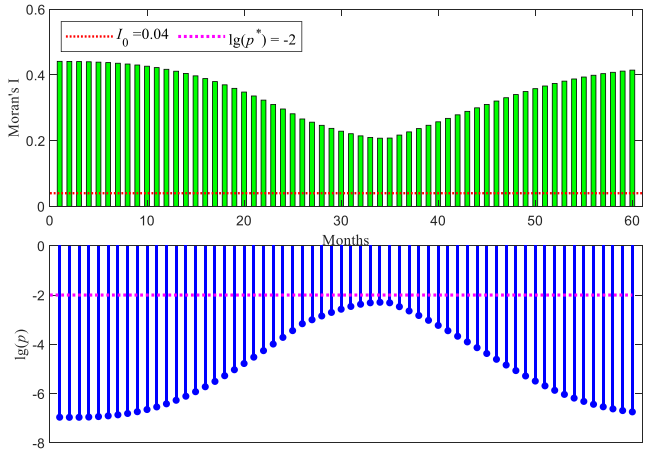

Fig. 3. Moran's I test on trend components.

The other components, as plotted in the bottom right of Fig. 2, usually consist of complex nonlinear elements and high-frequency noise. Here, as highlighted in the Introduction, the deep learning methods can handle these high-frequency components [59].

2.3. STGM for trend forecasting

Considering the spatiotemporal dependence in the trend component of the PM2.5 time-series, an STGM is proposed. The STGM is inspired by the GM(1,1) model (useful for time series forecasting under limited information) in subsection 2.2.1, and the first-order spatial autoregressive model (suitable for spatial data) in subsection 2.2.2. The parameter estimation and time response function of the STGM is discussed in subsection 2.2.3.

2.3.1. GM(1,1) model

Let $x^{(0)} = (x^{(0)}(1), x^{(0)}(2), \cdots, x^{(0)}(n))$ be an original sequence of the observations, then $x^{(1)} = x^{(0)}\mathbf{A}$ is the accumulated generated sequence and $z^{(1)} = (z^{(0)}(2), z^{(0)}(3), \cdots, z^{(0)}(n)) = x^{(1)}\mathbf{B_1}$ is the background generated sequence, where $\mathbf{A}$ be the first order accumulated generated matrix [60] and $\mathbf{B_1}$ is the background generated matrix,

$$A = \begin{pmatrix} 1 & 1 & \cdots & 1 \\ 0 & 1 & \cdots & 1 \\ \vdots & \vdots & \ddots & \vdots \\ 0 & 0 & \cdots & 1 \end{pmatrix}_{n\times n}, \quad \mathbf{B_1} = \begin{pmatrix} 0.5 & 0 & \cdots & 0 & 0 \\ 0.5 & 0.5 & \cdots & 0 & 0 \\ 0 & 0.5 & \cdots & 0 & 0 \\ \vdots & \vdots & \ddots & \vdots & \vdots \\ 0 & 0 & \cdots & 0.5 & 0.5 \\ 0 & 0 & \cdots & 0 & 0.5 \end{pmatrix}_{(n-1)\times n}$$

GM(1,1) can be written as

$$x^{(0)}(k) + az^{(1)}(k) = b, \quad k = 2, 3, \cdots, n \tag{3}$$

where a is the development coefficient of the model, and b is the grey input of the model. Moreover, the whitenization differential equation of the GM(1, 1) model is given by Equation (4)

$$\frac{dx^{(1)}}{dt} + ax^{(1)} = b \tag{4}$$

For Equation (4), given the initial condition $x^{(1)}(1) = x^{(0)}(1)$, the solution to the GM(1,1) model is

$$\hat{x}^{(1)}(k) = \left(x^{(0)}(1) - \frac{b}{a}\right)e^{-a(k-1)} + \frac{b}{a} \tag{5}$$

Then, $\hat{x}^{(0)}$, the prediction of $x^{(0)}$, can be obtained using Equation (6)

$$\hat{x}^{(0)} = \hat{x}^{(1)}\mathbf{A}^{-1} \tag{6}$$

The GM(1,1) model is the most basic grey model used to characterize the discrete time series with an approximate differential equation. The GM(1,1) model and its extensions consider only the temporal dependence but rarely discuss spatial dependence in the dataset.

2.3.2. Spatial autoregressive model

Spatial dependence in a collection of sample data observations refers to the phenomenon that the observation at spatial unit i, $x_i^{(1)}$ depends on the other observations at location j ($i \neq j$). In short, $x_i^{(1)}$ can be stated as

$$x_i^{(1)} = f\left(x_j^{(1)}\right),\ i = 1, 2, ..., m \tag{7}$$

where f is a spatial dependence function. In the most general case, a weight matrix is used to depict this functional spatial dependence.

Definition 1. For any i, let w_{ij} be the measurement about the spatial influence of unit j ($j \neq i$) on spatial unit i, then matrix $\mathbf{W} = \{w_{ij}\}_{m\times m}$ is the spatial weight matrix.

The spatial weight matrix $\mathbf{W}$ is symmetric and always has zeros on the main diagonal by convention. In spatial analysis, a linear relationship based on $\mathbf{W}$ is applied to depict Equation (7) as the First-order spatial AutoRegressive (FAR) model.

Definition 2. The FAR model [61] is given by

$$X^{(1)} = \rho\mathbf{W}X^{(1)} + \varepsilon \tag{8}$$

where $X^{(1)} = (x_1^{(1)}, x_2^{(1)}, \cdots, x_m^{(1)})^T$, ρ is a regression parameter to be estimated, and $\varepsilon \sim N(0, \sigma^2 I_m)$ is the random spatial error. Equation (8) is also the basial spatial model, which attempts to explain the variation in $X^{(1)}$, as a linear combination of contiguous or neighboring units with no other explanatory variables.

2.3.3. STGM(1,1) model

From Fig. 4, GM(1,1) is a point time series forecast [62], and the FAR model depicts the spatial data. Inspired by GM(1,1) and the FAR model, this subsection proposes an STGM to manage the spatiotemporal data. Let $x_i^{(0)}(k)$ be an original observation in location i at moment k, then all the total original observations can be listed as matrix $X^{(0)}$ of Equation (9).

For the original spatiotemporal data matrix of Equation (9), let its accumulated generated data be $X^{(1)} = \{X_i^{(1)}(k)\}_{m\times n}$, where $x_i^{(1)}(k) = \sum_{j=1}^{k} x_i^{(0)}(j)$ denotes the accumulated generated observation in location i at moment k , $k = 2, 3, \cdots, n$. Then, $X^{(1)}$ is obtained using

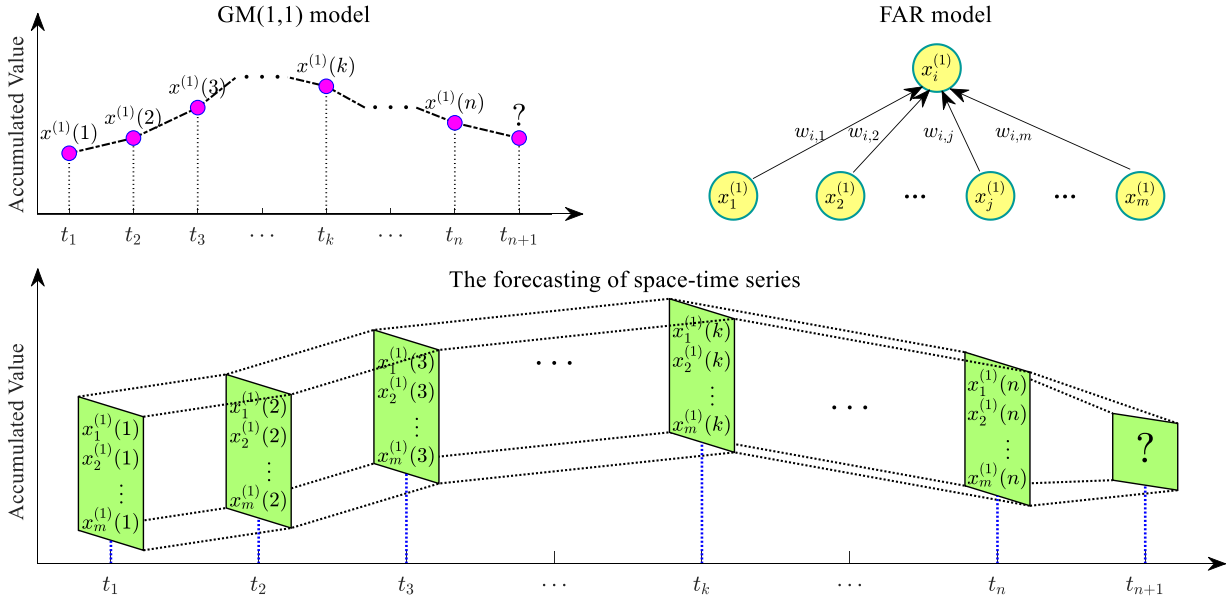

Fig. 4. Forecasting of space-time series.

$$X^{(0)} = \begin{pmatrix} x_1^{(0)}(1) & x_1^{(0)}(2) & \cdots & x_1^{(0)}(k) & \cdots & x_1^{(0)}(n) \\ x_2^{(0)}(1) & x_2^{(0)}(2) & \cdots & x_2^{(0)}(k) & \cdots & x_2^{(0)}(n) \\ \vdots & \vdots & \ddots & \vdots & \ddots & \vdots \\ x_i^{(0)}(1) & x_i^{(0)}(2) & \cdots & x_i^{(0)}(k) & \cdots & x_i^{(0)}(n) \\ \vdots & \vdots & \ddots & \vdots & \ddots & \vdots \\ x_m^{(0)}(1) & x_m^{(0)}(2) & \cdots & x_m^{(0)}(k) & \cdots & x_m^{(0)}(n) \end{pmatrix} \tag{9}$$

$$X^{(1)} = X^{(0)}\mathbf{A} \tag{10}$$

For spatial unit i, the time sequence $x_i^{(1)}$ has been characterized through the GM(1,1) whitenization of Equation (4) when considering the continuous temporal dependence. As shown in the upper right of Fig. 2, the spatial sequence, $X^{(1)}(k)$, can be formulized with the FAR model (8) from a spatial viewpoint at moment k. By considering both temporal and spatial dependence, this paper constructs the spatiotemporal differential equation (11) for the STGM(1,1) model while ignoring the spatial error ε as follows.

Definition 3. The spatiotemporal differential equation (11) is labeled as the whitenization differential equation of STGM(1,1), with

$$\frac{dX^{(1)}(t)}{dt} + \mathbf{a}\mathbf{W}X^{(1)}(t) = \mathbf{b} \tag{11}$$

where $X^{(1)}(t)$ is a sequence of functions, namely $X^{(1)}(t) = (x_1^{(1)}(t), x_2^{(1)}(t), \cdots, x_m^{(1)}(t))^T$, $x_i^{(1)}(t)$ is the accumulated value of spatial unit i at time t, $\mathbf{a} = diag(a_1, a_2, \cdots, a_m)$, $\mathbf{W}$ is the spatial weight matrix, and $\mathbf{b} = (b_1, b_2, \cdots, b_m)^T$. For spatial unit i, a_i is the spatial development coefficient and b_i is the grey input. According to Equation (11), the rate of change of the cumulative consumption [63] $x^{(1)}(t)$ in the period $[k-1, k]$ can be approximated as:

$$\frac{dX^{(1)}(t)}{dt}\Big|_{t=k} \approx \frac{\Delta X^{(1)}(t)}{\Delta t}\Big|_{t=k} = \frac{X^{(1)}(k) - X^{(1)}(k-1)}{k-(k-1)} = X^{(1)}(k) - X^{(1)}(k-1) = X^{(0)}(k) \tag{12}$$

It is worth noting that $X^{(0)}(k)$ is usually regarded as the grey derivative, which can yield the necessary information about $X^{(1)}(t)$. In short, $X^{(0)}(k)$ can approximate $\frac{dX^{(1)}(t)}{dt}$ in the period $[k-1, k]$. Further, the background value of this grey derivative [64] can be written as Equation (13):

$$X^{(1)}(t)|_{[k-1,k]} \approx 0.5X^{(1)}(k) + 0.5X^{(1)}(k-1), \quad k = 2, 3, \cdots, n. \tag{13}$$

Let $Z^{(1)}(k) = 0.5X^{(1)}(k) + 0.5X^{(1)}(k-1)$ be the background generated sequence expressed as

$$Z^{(1)} = \begin{pmatrix} z_1^{(0)}(2) & z_1^{(0)}(3) & \cdots & z_1^{(0)}(k) & \cdots & z_1^{(0)}(n) \\ z_2^{(0)}(2) & z_2^{(0)}(3) & \cdots & z_2^{(0)}(k) & \cdots & z_2^{(0)}(n) \\ \vdots & \vdots & \ddots & \vdots & \ddots & \vdots \\ z_i^{(0)}(2) & z_i^{(0)}(3) & \cdots & z_i^{(0)}(k) & \cdots & z_i^{(0)}(n) \\ \vdots & \vdots & \ddots & \vdots & \ddots & \vdots \\ z_m^{(0)}(2) & z_m^{(0)}(3) & \cdots & z_m^{(0)}(k) & \cdots & z_m^{(0)}(n) \end{pmatrix} = X^{(0)}AB_1 \tag{14}$$

In grey modeling, the background sequence $Z^{(1)}(k)$, can usually take the place of the sequence about $X^{(1)}(t)$ in the period $[k-1, k]$ [65]. Hence, we can define the following grey model.

Definition 4. Equation (15) defines STGM(1,1)

$$X^{(0)}(k) + \mathbf{a}\mathbf{W}Z^{(1)}(k) = \mathbf{b}, \quad k = 2, 3, \cdots, n \tag{15}$$

where $X^{(0)}(k) = (x_1^{(0)}(k), x_2^{(0)}(k), \cdots, x_m^{(0)}(k))^T$, $Z^{(1)}(k) = (z_1^{(0)}(k), z_2^{(0)}(k), \cdots, z_m^{(0)}(k))^T$. In Equation (15), $\mathbf{a}$ and $\mathbf{b}$ are the parameter matrices to be estimated.

For spatial unit i, its parameters, $P_i = (a_i, b_i)$, can be estimated through Theorem 1, which provides an estimation method for P_i.

Theorem 1. If $P_i = (a_i, b_i)^T$ is a parameter sequence , and $\mathbf{W}_{i,\cdot} = (w_{i,1}, w_{i,2}, \cdots, w_{i,m})$, with

$$B_i = \begin{bmatrix} -\mathbf{W}_{i,\cdot}z_i^{(1)}(2) & 1 \\ -\mathbf{W}_{i,\cdot}z_i^{(1)}(3) & 1 \\ \vdots & 1 \\ -\mathbf{W}_{i,\cdot}z_i^{(1)}(n) & 1 \end{bmatrix}, \quad Y_i = \begin{bmatrix} x_i^{(0)}(2) \\ x_i^{(0)}(3) \\ \vdots \\ x_i^{(0)}(n) \end{bmatrix}$$

then, $\widehat{P}_i = (\widehat{a}_i, \widehat{b}_i)^T$, and the least squares estimation of P_i satisfies

$$\widehat{P}_i = \left(B_i^T B_i\right)^{-1} B_i^T Y \tag{16}$$

Proof. For spatial unit i, putting $-z_i^{(1)}(k)$ into Equation (14) yields

$$\begin{aligned} x_i^{(0)}(2) &= -a_i z_i^{(1)}(2) + \rho_i \mathbf{W}_{i,\cdot}Z_i^{(1)}(2) + b_i \\ x_i^{(0)}(3) &= -a_i z_i^{(1)}(3) + \rho_i \mathbf{W}_{i,\cdot}Z_i^{(1)}(3) + b_i \\ &\vdots \\ x_i^{(0)}(n) &= -a_i z_i^{(1)}(n) + \rho_i \mathbf{W}_{i,\cdot}Z_i^{(1)}(n) + b_i. \end{aligned}$$

This is $Y_i = B_i P_i$ in matrix form. For the estimation value of the reference sequences P_i, using $-a_i\mathbf{W}_{i,\cdot}Z_i^{(1)}(k) + b$ instead of $x_i^{(0)}(k)$, $(k = 2, 3, \cdots, n)$ on the left-hand side, we obtain the sequence $\varepsilon_i = Y_i - B_i P_i$. Suppose

$$\begin{aligned} s_i &= \varepsilon_i^T \varepsilon_i = (Y_i - B_i P_i)^T (Y_i - B_i P_i) \\ &= \sum_{k=2}^{n} \left(x_i^{(0)}(2) + a_i \mathbf{W}_{i,\cdot}Z_i^{(1)}(2) - b_i\right)^2 \end{aligned}$$

Then, the parameter sequence $(\widehat{a}_i, \widehat{b}_i)^T$ that minimizes s should satisfy

$$\begin{cases} \dfrac{\partial s_i}{\partial a_i} = 2\sum_{k=2}^{n}\left(x_i^{(0)}(k) + \widehat{a}_i\mathbf{W}_{i,\cdot}Z_i^{(1)}(k) - \widehat{b}_i\right)\left(\mathbf{W}_{i,\cdot}Z_i^{(1)}(k)\right) = 0 \\ \dfrac{\partial s_i}{\partial b_i} = 2\sum_{k=2}^{n}\left(x_i^{(0)}(k) + \widehat{a}_i\mathbf{W}_{i,\cdot}Z_i^{(1)}(k) - \widehat{b}_i\right)\cdot(-1) = 0 \end{cases}$$

Therefore

$$\begin{cases} \sum_{k=2}^{n}\left(x_i^{(0)}(k) + \widehat{a}_i\mathbf{W}_{i,\cdot}Z_i^{(1)}(k) - \widehat{b}_i\right)\left(\mathbf{W}_{i,\cdot}Z_i^{(1)}(k)\right) = 0 \\ \sum_{k=2}^{n}\left(x_i^{(0)}(k) + \widehat{a}_i\mathbf{W}_{i,\cdot}Z_i^{(1)}(k) - \widehat{b}_i\right) = 0 \end{cases}$$

The above equations are then converted into matrix form, namely,

$$B_i^T(Y_i - B_i\widehat{P}_i) = 0$$

Thus, $B_i^T B_i \widehat{P}_i = B_i^T Y_i$ and $(B_i^T B_i)^{-1} B_i^T B_i \widehat{P}_i = (B_i^T B_i)^{-1} B_i^T Y_i$, proving Theorem 1.

Next, we discuss the unbiasedness of this method.

Theorem 2. Suppose $\varepsilon_{i,k} = x_i^{(0)}(k) + a_i\mathbf{W}_{i,\cdot}Z_i^{(1)}(k) - b_i$, $\forall k \in \{2, 3, \cdots, n\}$ with ε_i independent and identically distributed and $E(\varepsilon_{i,k}) = 0$, then $E(\widehat{P}) = P_i$.

Proof. Clearly,

$$E(\widehat{P}_i) = E\left(\left(B_i^T B_i\right)^{-1} B_i^T Y_i\right) = E\left(\left(B_i^T B_i\right)^{-1} B_i^T (B_i P_i + \varepsilon_i)\right)$$
$$= E\left(\left(B_i^T B_i\right)^{-1} B_i^T B_i P_i + \left(B_i^T B_i\right)^{-1} B_i^T \varepsilon_i\right)$$
$$= P_i + E\left(\left(B_i^T B_i\right)^{-1} B_i^T \varepsilon_i\right) = P_i + \left(B_i^T B_i\right)^{-1} E\left(B_i^T \varepsilon_i\right)$$

As

$$\frac{dX^{(1)}(t)}{dt} = \frac{de^{\mathbf{\Lambda} t}}{dt}\mathbf{c}(t) + e^{\mathbf{\Lambda} t}\frac{d\mathbf{c}(t)}{dt} = \mathbf{\Lambda} X^{(1)}(t) + e^{\mathbf{\Lambda} t}\frac{d\mathbf{c}(t)}{dt} = \mathbf{\Lambda} X^{(1)}(t) + \mathbf{b}.$$

Then $\frac{d\mathbf{c}(t)}{dt} = e^{-t\mathbf{\Lambda}}\mathbf{b}$,

$$\mathbf{c}(t) = \int_1^t e^{-u\mathbf{\Lambda}}\mathbf{b}\,du + \mathbf{c}(1) = \left(e^{-t\mathbf{\Lambda}} - e^{-\mathbf{\Lambda}}\right)\mathbf{\Lambda}^{-1}\mathbf{b} + e^{-\mathbf{\Lambda}}X^{(0)}(1).$$

Thus

$$\widehat{X}^{(1)}(t) = e^{\mathbf{\Lambda} t}\mathbf{c}(t) = e^{\mathbf{\Lambda} t}\left[\left(e^{-t\mathbf{\Lambda}} - e^{-\mathbf{\Lambda}}\right)\mathbf{\Lambda}^{-1}\mathbf{b} + e^{-\mathbf{\Lambda}}X^{(0)}(1)\right] = \mathbf{\Lambda}^{-1}\mathbf{b} + e^{\mathbf{\Lambda}(t-1)}\left[X^{(1)}(1) - \mathbf{\Lambda}^{-1}\mathbf{b}\right].$$

$$E\left(B_i^T \varepsilon_i\right) = E\begin{pmatrix}\sum_{k=2}^{n} \mathbf{W}_{i,\cdot} Z^{(1)}(k)\varepsilon_{i,k} \\ \sum_{k=2}^{n} \varepsilon_{i,k}\end{pmatrix} = \begin{pmatrix}\sum_{k=2}^{n} \mathbf{W}_{i,\cdot} Z^{(1)}(k) E(\varepsilon_{i,k}) \\ \sum_{k=2}^{n} E(\varepsilon_{i,k})\end{pmatrix} = \begin{pmatrix}0 \\ 0\end{pmatrix},$$

the Proof follows.

Theorem 2 asserts that the least-squares estimate of STGM(1,1) is unbiased. After estimating $P_i = (a_i, b_i)^T$ using Theorem 1, the parameters matrices $\mathbf{a}$, $\boldsymbol{\rho}$, and $\mathbf{b}$ in Equation (12) can be obtained and the solution to Equation (12) follows.

Theorem 3. Let the initial sequence be $X^{(1)}(1) = X^{(0)}(1)$. The time response function sequence of Equation (12) is then given by

$$\widehat{X}^{(1)}(t) = e^{(t-1)\mathbf{\Lambda}}\left[X^{(1)}(1) - \mathbf{\Lambda}^{-1}\mathbf{b}\right] + \mathbf{\Lambda}^{-1}\mathbf{b} \tag{17}$$

where $\mathbf{\Lambda} = -\mathbf{aW}$, $e^{(t-1)\mathbf{\Lambda}} = \mathbf{V}\begin{pmatrix} e^{\lambda_1(t-1)} & 0 & \cdots & 0 \\ 0 & e^{\lambda_2(t-1)} & \cdots & 0 \\ \vdots & \vdots & \ddots & \vdots \\ 0 & 0 & \cdots & e^{\lambda_m(t-1)} \end{pmatrix}\mathbf{V}^{-1}$,

and $\mathbf{V} = (V_1, V_2, \cdots, V_n)^T$, V_i is an eigenvector of $\mathbf{\Lambda}$ and λ_i is the corresponding eigenvalue. *Proof.* As $\mathbf{\Lambda} = -\mathbf{aW}$, the spatiotemporal differential equation, Equation (12), can be rewritten as

$$\frac{dX^{(1)}(t)}{dt} = \mathbf{\Lambda} X^{(1)}(t) + \mathbf{b} \tag{18}$$

Suppose $X^{(1)}(t) = e^{\mathbf{\Lambda} t}\mathbf{c}(t)$ and $X^{(1)}(1) = X^{(0)}(1)$. Then $X^{(1)}(1) = e^{\mathbf{\Lambda}}\mathbf{c}(1) = X^{(0)}(1)$, i.e., $\mathbf{c}(1) = e^{-\mathbf{\Lambda}}X^{(0)}(1)$

The Proof of Theorem 3 is now complete.

Theorem 3 provides a time response function sequence for STGM (1,1), the original observation sequence can be predicted using the reduced form

$$\widehat{X}^{(0)} = \widehat{X}^{(1)}\mathbf{A}^{-1}. \tag{19}$$

2.4. LSTM for daily remainder forecasting

As the remainder component usually consists of complex nonlinear elements and noise, this paper uses the LSTM network to forecast this component.

The LSTM network is a recurrent neural network [66]. By treating the hidden layer as a memory unit, the LSTM network can handle the correlation within the time series in both short and long term. In this paper, the structure of the memory unit is shown in Fig. 5. The LSTM prediction model can be established directly by using the Keras deep learning package in MATLAB 2017b [67]. The input layer of the trained LSTM network has 9 features and 11 time steps; the hidden neurons were set to 10. The output layer with linear activation function has one neuron. The maximum number of epochs were set at 50.

2.5. PM2.5 forecasting model

The exact combined model of the STGM and LSTM network (STGM-LSTM) can be expressed as Equation (20), namely,

$$y_{i,k,d} = s_i(k) + x_i^{(0)}(k) + e_{i,k,d} \tag{20}$$

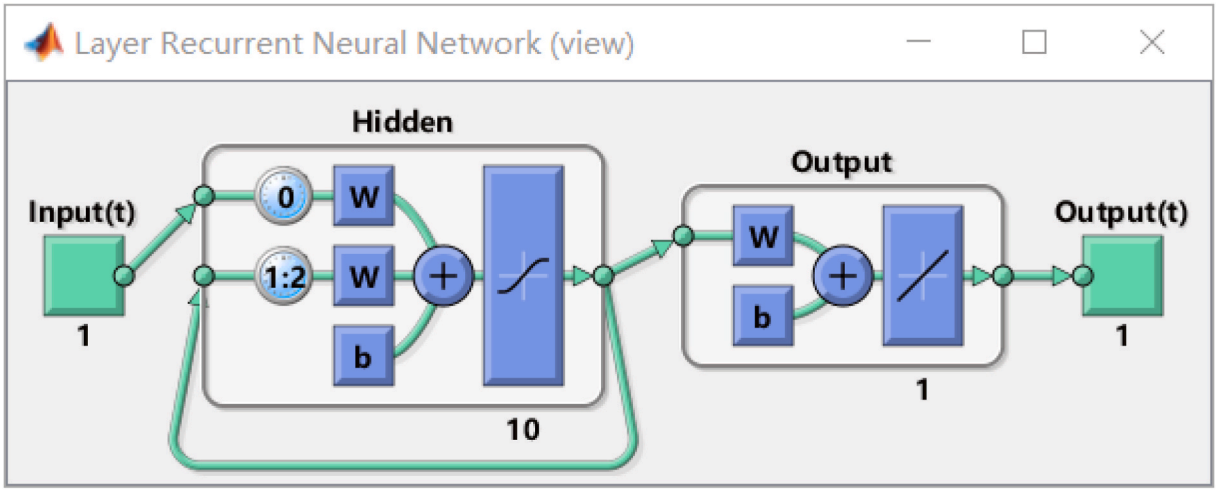

Fig. 5. Structure of LSTM

where,

$s_i(k)$←Yearly periodic constant.
$x_i^{(0)}(k)$←STGM(1, 1)
$e_{i,k,d}$←LSTM model,

and,

$$\begin{cases} X^{(0)} = \left\{x_i^{(0)}(k)\right\}_{m\times n} \\ \widehat{P}_i = \left(B_i^T B_i\right)^{-1} B_i^T Y \\ \widehat{X}^{(1)}(t) = e^{(t-1)\mathbf{\Lambda}}\left[X^{(1)}(1) - \mathbf{\Lambda}^{-1}\mathbf{b}\right] + \mathbf{\Lambda}^{-1}\mathbf{b} \\ \widehat{X}^{(0)} = \widehat{X}^{(1)}\mathbf{A}^{-1}. \end{cases}$$

The steps of this combined model are as follows:

Step 1. Collect the original data space-time series $y_{i,k,d}$. Split $s_i(k)$ and $x_i^{(0)}(k)$ from $y_{i,k,d}$ using STL, and determine the remainder component based on Equation (2).

Step 2. Determine the spatial weight matrix W, and test W based on Moran's I test.

Step 3. Form the accumulated generated observation matrix $X^{(1)}$, and construct parameter matrix B. Based on the parameter estimation (Theorem 1, or Equation (16)), estimate the model parameters $\widehat{P}_i = (a_i, b_i)^T$.

Step 4. Find the model prediction value sequence $\widehat{X}^{(1)}$ based on Equation (17), to obtain the model reduction value sequence $\widehat{X}^{(0)}(t)$ based on Equation (18).

Step 5. Forecast the remainder component using LSTM, and form the forecast of $y_{i,k,d}$.

Step 6. Verify the results and analyze the errors of this model.

3. Validation

In this section, the advantages of STGM(1,1) over the existing GM (1,1) and the space-time series forecasting model are demonstrated using the five forecast accuracy metrics of Section 3.1. In Section 3.2, the grey space-time series datasets are used to validate the prediction performance of STGM(1,1).

3.1. Forecast accuracy metrics

Five metrics: Mean Absolute Percentage Error (MAPE), Mean Absolute Deviation (MAD), Standard deviation of absolute percentage error (STD), R-squared (R^2), and Index of Agreement (IA) are used to validate the models. The five metrics are as shown:

$$\text{MAPE} = \frac{1}{m(n-1)}\sum_{i=1}^{m}\sum_{k=2}^{n}\frac{\left|\widehat{x}_i^{(0)}(k) - x_i^{(0)}(k)\right|}{x_i^{(0)}(k)} \times 100\% \tag{21}$$

$$\text{RMSE} = \sqrt{\frac{1}{m(n-1)}\sum_{i=1}^{m}\sum_{k=2}^{n}\left(\widehat{x}_i^{(0)}(k) - x_i^{(0)}(k)\right)^2} \tag{22}$$

$$\text{STD} = \sqrt{\frac{1}{m(n-1)}\sum_{i=1}^{m}\sum_{k=2}^{n}\left(\frac{\left|\widehat{x}_i^{(0)}(k) - x_i^{(0)}(k)\right|}{x_i^{(0)}(k)} - \text{MAPE}\right)^2} \tag{23}$$

$$R^2 = 1 - \frac{\sum_{i=1}^{m}\sum_{k=2}^{n}\left(\widehat{x}_i^{(0)}(k) - x_i^{(0)}(k)\right)^2}{\sum_{i=1}^{m}\sum_{k=2}^{n}\left(\widehat{x}_i^{(0)}(k) - \overline{x}_i^{(0)}\right)^2} \tag{24}$$

$$\text{IA} = 1 - \frac{\sum_{i=1}^{m}\sum_{k=2}^{n}\left(\widehat{x}_i^{(0)}(k) - x_i^{(0)}(k)\right)^2}{\sum_{i=1}^{m}\sum_{k=2}^{n}\left(\left|\widehat{x}_i^{(0)}(k) - \overline{x}_i^{(0)}\right| + \left|x_i^{(0)}(k) - \overline{x}_i^{(0)}\right|\right)^2} \tag{25}$$

where $\overline{x}^{(0)}$ is the average of the training data, and $\overline{x}_i^{(0)} = \frac{1}{n-1}\sum_{k=2}^{n} x_i^{(0)}(k)$.

Table 2
Summary of results of fitting and prediction about the grey space-time series datasets[a].

Metric		STGM	MGM	GM(1,1)	STARMA	ARIMA
Fitting						
MAPE	Max.	**3.39%**	13.31%	22.53%	37.49%	552.51%
	Avg.	**1.34%**	3.77%	9.54%	23.88%	47.56%
	Std.	**0.74%**	5.14%	3.40%	6.73%	84.49%
STD	Max	**3.61%**	6.45%	20.08%	16.20%	839.84%
	Avg.	**1.34%**	2.59%	10.27%	8.81%	50.51%
	Std.	**2.71%**	6.96%	9.92%	9.05%	38.25%
Prediction						
MAPE	Max.	**10.09%**	32.51%	47.86%	51.46%	190.00%
	Avg.	**4.02%**	10.18%	14.82%	22.87%	44.37%
	Std.	**0.77%**	1.30%	3.45%	3.33%	133.14%
STD	Max.	**8.14%**	18.62%	24.51%	25.51%	194.60%
	Avg.	**2.42%**	3.94%	10.47%	5.87%	28.12%
	Std.	**1.64%**	3.67%	4.89%	5.60%	30.51%[a]

[a] Note: Max. means the maximum value of results, Avg. means the average value of results, and Std. means the standard deviation of results.

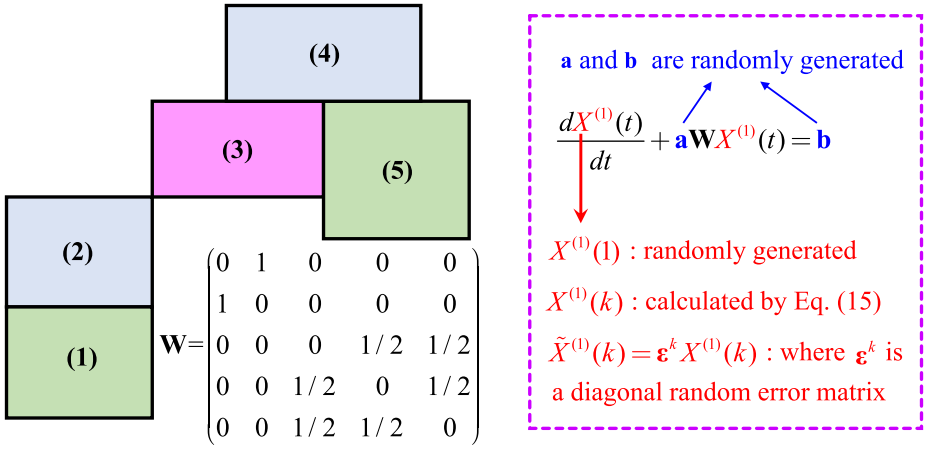

Fig. 6. Generator of grey space-time series datasets.

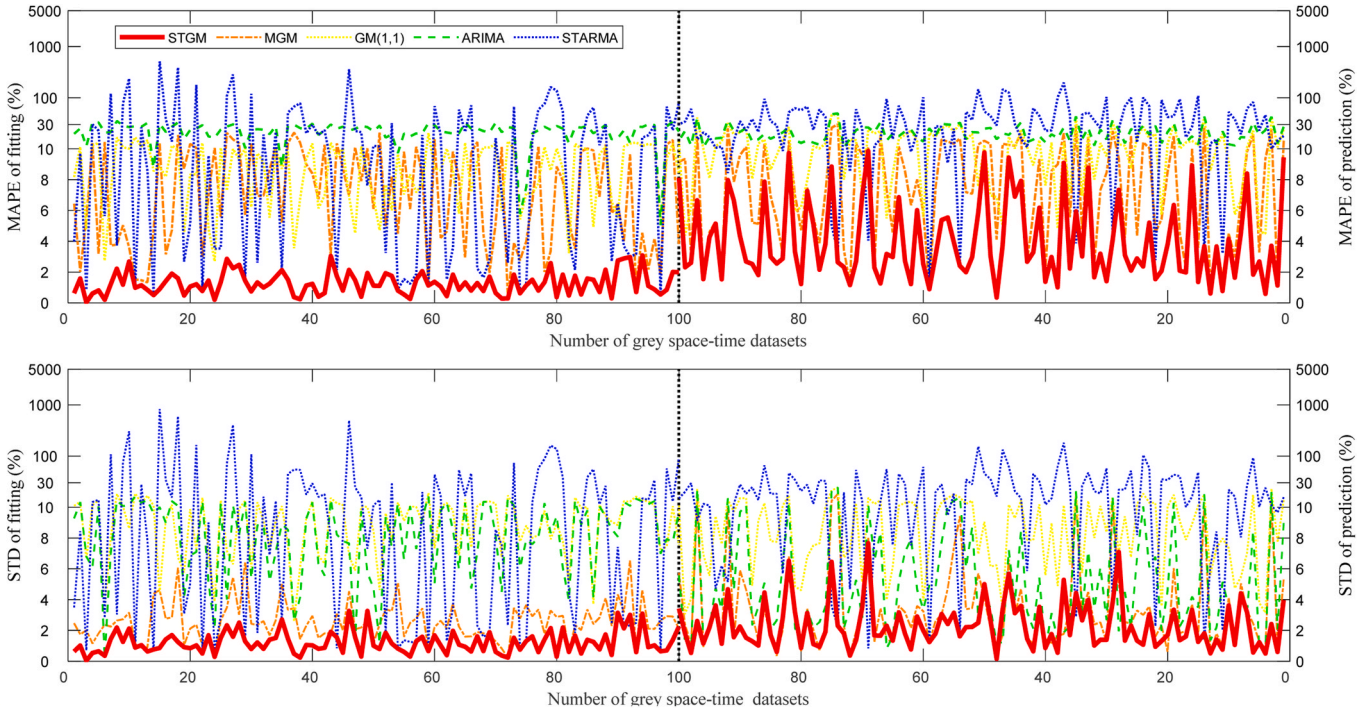

Fig. 7. MAPE and STD of various forecasting models on grey space-time datasets.

3.2. Validating STGM (1,1)

To evaluate the impact of the spatial dependence in the grey modeling, an ablation validation is designed in this subsection. As STGM (1,1) is established using spatial and temporal dependence, we design the validation about the proposed model based on 100 grey space-time series datasets.

As shown in Fig. 6, the major parameter matrix of the spatiotemporal differential Equation (9), W is a spatial weight matrix whose spatial structure is referred from the literature [68], with a and b being randomly generated. For m spatial units with a given length of time, N, a diagonal random matrix $\boldsymbol{\varepsilon}^k = diag(\varepsilon_1^k, \varepsilon_2^k, \cdots, \varepsilon_m^k)$ is designed to simulate the disturbance error at moment k, where ε_i^k $(i = 1, 2, \cdots, m\ k = 1, 2, \cdots, N)$ is uniformly distributed $\varepsilon_i^k \sim U(0.90, 1.10)$. Hence, we have a simulation observation matrix, $\widetilde{X}^{(1)} = \{\widetilde{x}_i^{(1)}(k)\}_{m\times N}$, and its corresponding original modeling observation matrix, $\widetilde{X}^{(0)} = \{\widetilde{x}_i^{(0)}(k)\}_{m\times N}$, where N is a pseudorandom scalar integer $N \in [12, 24]$.

The STGM results are compared against four models, i.e., GM(1,1) without spatial dependence, multi-variable grey model (MGM) [69], ARIMA, and STARMA [70]. The metrics, MAPE and STD, are used to evaluate these results. Table 2 lists the summary of the results. (The average and max of the RMSE are not listed since this metric depends on the order of the magnitude of the training data). All of the detailed data and corresponding model results are placed as supplementary material.

STGM always yields the best performance both in the fitting and prediction of these grey space-time series datasets. As shown in Table 2, STGM has the smallest MAPE and STD (marked with bold font) both in fitting and prediction, which means that STGM has the best performance on precision and robustness. Fig. 7, which shows the detailed result of the grey space-time datasets, supports this outcome. In Fig. 7, both the MAPE and STD of STGM lie at the bottom, regardless of fitting or prediction.

As expected, the design of spatial dependence helps to weaken the disturbance effect, which is necessary in STGM(1,1). From Table 2 and Fig. 7, all metrics of STGM(1,1) are better than those of MGM(1,N) and GM(1,1), which do not characterize the spatial weight matrix. Further, STARMA performs better than the ARIMA model, which assumes that

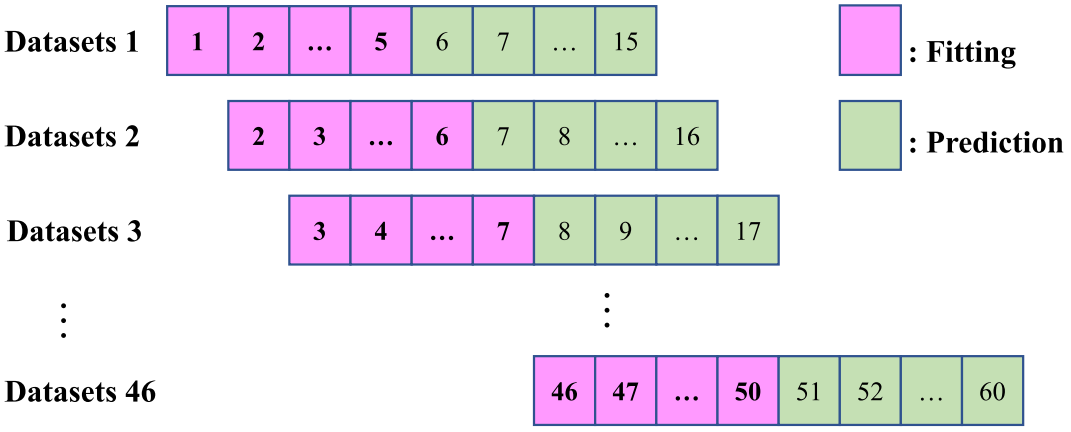

Fig. 8. Remaining components of PM2.5 time series.

Table 3
Comparison of STGM-LSTM against other models on forecasting PM2.5 time series.

Metric		STGM-LSTM	STARMA-LSTM	STGM-Elman	STGM-LSSVM	STGM-GRNN
Fitting						
RMSE	Max.	10.196	19.969	32.720	**6.226**	34.183
	Avg.	1.187	5.534	13.841	**1.078**	6.555
STD	Max.	18.294	21.818	27.476	**12.604**	37.191
	Avg.	2.139	3.781	13.151	**1.185**	7.222
R2	Min.	**0.896**	0.834	0.733	0.817	0.899
	Avg.	**0.983**	0.916	0.850	0.927	0.924
IA	Min.	**0.950**	0.884	0.770	0.796	0.722
	Avg.	**0.993**	0.925	0.860	0.903	0.864
Prediction						
RMSE	Max.	**46.93**	75.96	128.71	146.68	131.86
	Avg.	**29.14**	42.54	77.58	48.21	58.19
STD	Max.	**32.57**	83.46	112.41	84.73	134.71
	Avg.	**19.94**	46.70	61.84	45.44	71.14
R2	Min	**0.721**	0.659	0.579	0.720	0.710
	Avg.	**0.744**	0.723	0.672	0.732	0.729
IA	Min.	**0.740**	0.698	0.608	0.628	0.720
	Avg.	**0.748**	0.730	0.679	0.679	0.682

the spatial units are independent. Thus, including spatial dependence helps to improve the model's precision. Moreover, STGM(1,1) behaves better than STARMA, which is absent from the design of the dynamic differential equation. At the same time, GM(1,1) has a smaller MAPE and STD than the ARIMA model. Thus, it is worthwhile to consider spatial dependence to attenuate the disturbance error and improve the precision and robustness of the model.

3.3. Validation using historical PM2.5 space-time series

In this section, the historical space-time series dataset about PM2.5 in WMA (from 1 Jan 2015 to 31 Dec 2019) are collected to validate the proposed method. The data cover 26 observation sites over 60 months. Through STL decomposition, the trend and remainder components are extracted from the original data in Fig. 2. Then, as shown in Fig. 8, these components are continuously rolling and spilt into 46 datasets to avoid the contingency in a single validation.

For each group of datasets, the first 5 months are used as the training data for estimating the parameters and for building the model. The rest of the data from the last 10 months are used to test the model. Thus, 46 STGM-LSTM models are formed for each dataset.

The results are compared against other combination models, including STARMA-LSTM, STGM-Elman (STGM combined with the Elman neural network model), STGM-LSSVM (STGM combined with the Least Squares SVM), STGM-GRNN (STGM combined with the general regression neural network). The RMSE, STD, R^2, and IA of the model outcomes against the actual values are listed in Table 3.

All the criteria of STGM-LSTM for prediction fare better than those of STARMA-LSTM, STGM-Elman, STGM-LSSVM, and STGM-GRNN, suggesting that STGM-LSTM has the highest prediction accuracy and stability. The results also inform that the metrics of STGM-LSSVM are ideal for fitting. The prediction of STGM-LSTM ranks first, followed by the fitting results. The ranking for the prediction effect of STARMA-LSTM ranks second, and the fitting effect ranks third. The R^2 obtained by STGM-LSTM is close to the actual data. In conclusion, STGM-LSTM is the best method for validating the 46 datasets. Thus, this novel combined model is a potential approach for the mid-long forecast of PM2.5 concentration.

4. Application

In this section, the daily PM2.5 emissions in Wuhan during the lockdown and post-pandemic period are predicted using STGM-LSTM. The momentum and spillover effects of the lockdown policy are measured by comparing with the actual observations.

4.1. PM2.5 concentration forecast during lockdown

As the combined STGM-LSTM model has shown potential for mid to long term forecasting of PM2.5 concentration in subsection 3.3, this paper applied this model to forecast the PM2.5 concentration during the lockdown based on the historical training data (from 1 August to 31 December 2019), which is plotted as a solid blue line in Fig. 9.

To compare the forecasts, the historical PM2.5 concentration (from 23 January to 7 April 2019, marked with a solid green line) and the actual value (from 23 January to 7 April 2020, marked with a solid red line) are plotted in Fig. 9. The average daily PM2.5 of the six main cities of WMA are plotted on the left of Fig. 9.

The left of Fig. 7 shows that there is a spatial effect in the PM2.5 concentration of these cities. As shown in Fig. 1, the observation sites in Huanggang are closer to those in Ezhou than the others. Thus, the curves of Huanggang are similar to those of Ezhou. This suggests that there

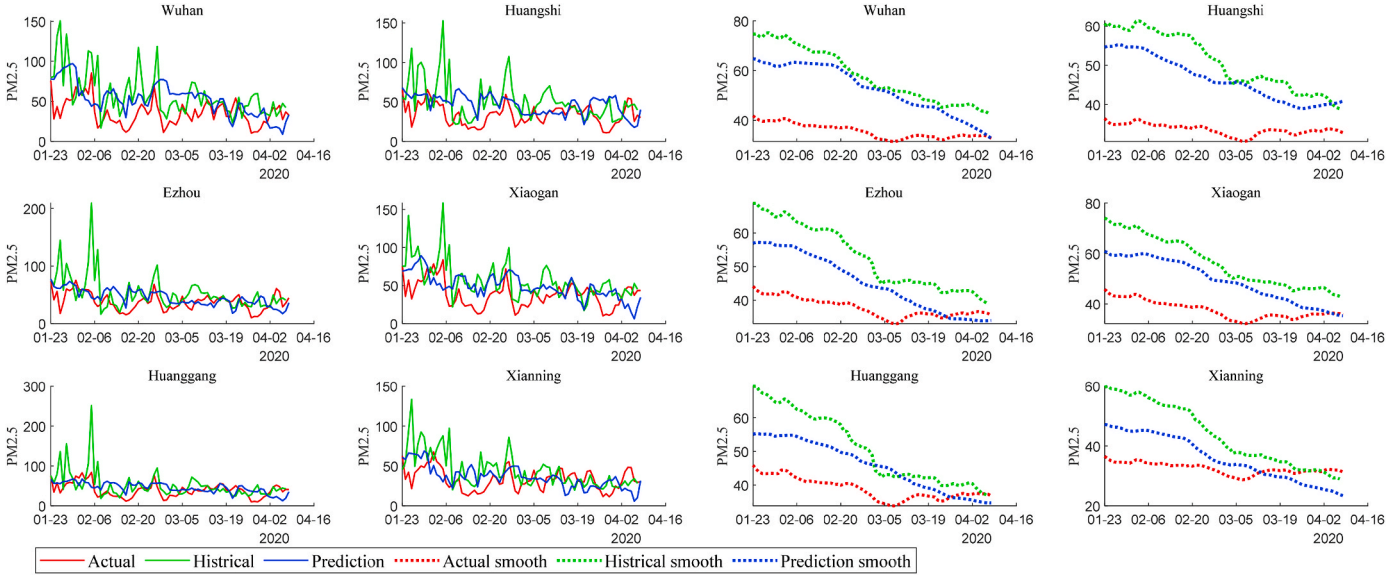

Fig. 9. PM2.5 concentration forecast during lockdown.

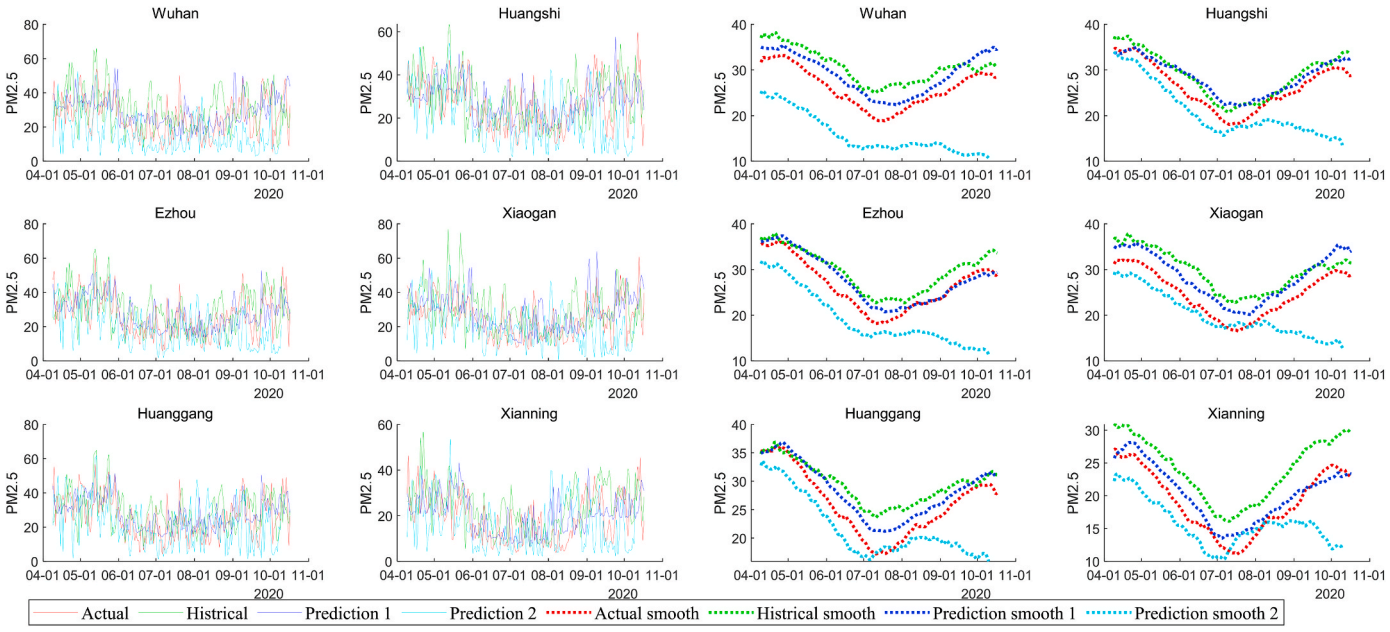

Fig. 10. PM2.5 concentration forecast during post-pandemic period.

exists a spatial effect in PM2.5 concentration observations. Further, there is now some rationale for adopting a spatial model for forecasting PM2.5.

Initiating a stringent lockdown has a positive effect on reducing the concentration of PM2.5. To improve the readability of these subplots, the daily curves are smoothed with the local *k*-point moving average operator and marked with the dashed line in the right of Fig. 9. From the smoothed curves, it is noted that the red dashed lines are invariably at the bottom, suggesting that the actual concentration of PM2.5 is at the lowest level. With the end of the lockdown, the red line converges to the green and blue lines, implying that the improvement in the concentration of PM2.5 due to the lockdown policies is weakening. These results suggest that the lockdown policies have a significant spillover effect on reducing the PM2.5 concentration, concurring with Zheng et al. (2020) [71].

Efforts by the community can also help to promote the reduction in PM2.5 concentration. The blue lines are the forecast of PM2.5 based on the training data from the pre-pandemic period. They are also regarded as the estimation of PM2.5 concentration where COVID-19 and the lockdown would not have happened. From Fig. 9, the forecast curves are almost lower than the historical curves for the same period in 2019, suggesting that the social efforts from the pre-pandemic period might lend a downward momentum to the PM2.5 concentration. This observation is supported by the fact that the local government carried out many landscaping projects for the Military World Games in 2019, thereby improving the air quality since then.

4.2. PM2.5 concentration forecasting after pandemic

For the post-pandemic period, this paper collected the latest PM2.5 concentration data (from 9 April to 17 October 2020), which are plotted with a solid red line in Fig. 10. To analyze the influence of the historical and the lockdown policies, this paper forecasts the PM2.5 concentration based on the training data from 1 August to 31 December 2019 (Prediction 1, marked with a solid blue line) and the training data from 8 December 2019 (when the first case is reported in literature [72]) until 8 April 2020 (Prediction 2, marked in solid cyan). The PM2.5 concentration during the same period of 2019 is labeled as the historical value, which is a solid green line in Fig. 10. Similarly, the daily curves are smoothed using a local moving average operator and marked by a dashed line on the right of Fig. 10.

Social efforts in a pre-pandemic period appear to lend a positive momentum effect in lowering the concentration of PM2.5 after the pandemic. From the smoothed curves, it is noted that the blue dashed lines are generally below the green dashed lines. As Prediction 1 is based on pre-pandemic training data, which only takes into account the social efforts pre-pandemic, this suggests that social efforts have a positive momentum in lowering PM2.5 concentration.

The lockdown has a further momentum effect on decreasing PM2.5 concentration. As shown in the right of Fig. 10, the red dash lines are generally below the blue or green dash lines. The red dash lines are obtained from the solid red curves, which is the actual PM2.5 concentration. As the actual PM2.5 concentration is influenced by past social efforts and the lockdown policies, the momentum effect of a lockdown will continue to promote the reduction in PM2.5 concentration even after a lockdown. However, the red dash curves converge to the blue dash curves after August 2020, suggesting that the momentum effect of these lockdown policies may disappear, allowing PM2.5 pollution to rebound, a sign of economic recovery.

Extending the lockdown period can keep the PM2.5 concentration at bay. The cyan curves (Prediction 2) are based on the training data from the lockdown period. Compared to the others, the cyan curves are always the lowest, which means that there will be more spillover effects from reducing the PM2.5 concentration if the lockdown period were to be extended.

These spillover effects are spatial heterogeneous. On the right of Fig. 10, the difference between the cyan and the other curves in Wuhan is always larger than those in the other cities, suggesting a greater spillover effect in Wuhan. This is due to the social structure or economic differences of these cities. Hence, the policies instituted during a lockdown should be tuned to local conditions notably the environmental and economic concerns.

4.3. Discussion

This study is an initial effort to understand how a pandemic lockdown can affect PM2.5 concentration. Compared with those in the same period of 2019, the PM2.5 concentration has significantly decreased in 2020, which is caused by the momentum effect of earlier social efforts and the spillover effect of the lockdown policies. The momentum and

Table 4
Momentum and spillover effects on PM2.5 concentration (in μg/m^3).

City		Wuhan	Huangshi	Ezhou	Xiaogan	Huanggang	Xianning
Lockdown period							
Historical period		58.72	51.39	53.39	57.16	51.74	44.39
Momentum effect 1	Prediction 1	52.28	46.47	45.14	49.13	45.44	36.10
	Reducing	6.44	4.92	8.25	8.03	6.29	8.29
	R.P.	10.97%	9.57%	15.45%	14.05%	12.17%	18.67%
Spillover effect	Actual	36.07	34.09	38.28	38.36	39.43	32.96
	Reducing	16.21	12.38	6.86	10.77	6.01	3.14
	R.P.	27.60%	24.09%	12.84%	18.84%	11.62%	7.07%
Post-pandemic period							
Historical period		30.56	28.77	29.55	29.52	29.29	23.98
Momentum effect 1	Prediction 1	29.17	28.41	27.81	28.56	28.17	20.36
	Reducing	1.39	0.36	1.74	0.96	1.12	3.62
	R.P.	4.55%	1.26%	5.89%	3.26%	3.81%	15.10%
Momentum effect 2	Actual	25.95	26.31	26.46	24.73	25.98	19.20
	Reducing	3.22	2.10	1.35	3.83	2.19	1.16
	R.P.	10.54%	7.29%	4.57%	12.97%	7.48%	4.82%
Spillover effect	Prediction 2	15.76	20.77	19.08	19.80	21.61	15.54
	Reducing	10.19	5.54	7.38	4.93	4.37	3.66
	R.P.	33.35%	19.25%	24.97%	16.69%	14.93%	15.27%

Note: R.P. refers to reducing percentage, which is the reduced value divided by the value in the historical period.

spillover effects are analyzed through a PM2.5 concentration forecast model (STGM-LSTM). The results are plotted in Figs. 9 and 10, and the momentum and spillover effects are quantified in Table 4.

From the results in subsections 4.1 and 4.2, the values of PM2.5 concentration during the lockdown and post-pandemic periods is averaged in Table 4. Compared to the same period in 2019 (the historical period), the values of the reduction caused by the momentum effect of past social efforts (labeled as Momentum effect 1) are obtained. Comparing the actual values with those of Prediction 1, the spillover of the lockdown are estimated in a lockdown period. During the post-pandemic period, the additional momentum effect of the lockdown policies (labeled as Momentum effect 2) are obtained using Prediction 2 less the actual values.

Benefiting from past social efforts before a lockdown, the PM2.5 concentration would drop by an average of 4.92–8.29 μg/m^3 during a lockdown. Comparing the forecast of PM2.5 concentration with the actual values, this paper estimates that the lockdown policies lowered the PM2.5 concentration reduce by 3.14–16.21 μg/m3, while the spillover effect of a lockdown varies from 7.07 to 27.60%, a function of the cities studied. Compared to the other cities, Wuhan has more industrial and vehicular traffic. As movement control is closely monitored during a lockdown, the PM2.5 from traffic pollution has thus reduced much more.

After the pandemic, the reduction in PM2.5 concentration arises from two momentum effects – (i) past social efforts which helped to reduce the concentration by 0.36–3.62 μg/m^3 (3.26–15.10% y-o-y), and (ii) lockdown which forced PM2.5 concentration to drop a further 1.16–3.22 μg/m^3 (or 4.57–12.97% compared to the same period in the previous year).

The additional spillover effect would be spatial heterogeneous if the lockdown were extended. This research discussed an additional spillover effect on improving the PM2.5 pollution. Comparing Prediction 2 with the actual, the additional spillover effect of a lockdown can lower PM2.5 by 3.66–10.19 μg/m^3. As these spillover effects are spatially heterogeneous, the lockdown policies should be adjusted based on economic and environmental considerations.

As the existing research emphasizes, the lockdown policies for COVID-19 usually have some unneglected influences on the air quality [73]. Quantitatively analyzing these influences using the grey spatiotemporal model and empirical data in WMA, this research discussed the spillover and momentum effect of the Lockdown on improving the PM2.5 pollution, where the momentum effect even sustained influence the air quality in the post-epidemic era. These effects can be explained from two following aspects.

On the one hand, the air pollution from industry is affected by the momentum effect of Lockdown, and fluctuates with the scale of production. The lockdown policies made the production and service of manufacturing in WMA have slowed down even standstill. And Wuhan's GDP during this period decreased by 40.5% comparing with the same period in history. Aiming at recovering the economic, the government of Wuhan raised 60 billion yuan (about $9.15 billion) and introduced 21 policies to help enterprises resume production [74]. These policies bring the industrial economy in steady recovery, the PM2.5 also slowly mushrooms as manufacturing production grow at the same time, which means the momentum effect of the Lockdown is gradually dying out.

On the other hand, the air pollution from traffic also is affected by the momentum effect. Although the daily traffic travel has been close to pre-epidemic levels since April 22th 2020, the COVID-19 still affects citizens' lifestyles. Office travel is dropped because many employees start to switch to remote work [75]. More relevantly, the falling of tourism demand reduces the related PM2.5 emission in the early post-epidemic era. Then this part of PM2.5 emission arises with the tourism recovery [76] in following period, which makes the momentum effect weaken.

5. Conclusion

This study analyses the trends in the PM2.5 concentration measured on the urban clusters around Wuhan in Hubei province during three periods: pre-pandemic, lockdown, and post-pandemic. Specifically, the study has delivered on the following:

(1) A novel spatiotemporal grey model considering the spatial effect of PM2.5 emission is proposed.
(2) Benefiting from the past social efforts before a pandemic, the PM2.5 concentration has declined by 4.92–8.29 μg/m^3 during a lockdown, and the reduction due to the momentum effect is 9.57–18.67%.
(3) Comparing the forecast of PM2.5 with the actual values, the lockdown policies lead to a further reduction in PM2.5 concentration of 3.14–16.21 μg/m^3, and the corresponding reduction due to the spillover effect of the lockdown is 7.07–27.60%.
(4) After the pandemic, PM2.5 concentration decreases by 0.36–3.62 μg/m^3 compared to the same period in 2019. The momentum effect of a lockdown has reduced the PM2.5 concentration by 1.16–3.83 μg/m^3.

The above results are constrained by the characteristics of the data and policy. As a system's behavior is influenced by the system factors, this would suggest that the system's behavior also carries the information about the factors [77]. Grey modeling usually constructs a forecasting model based on a univariate time series (behavior sequence). However, air pollution is a complex problem linked to multiple factors like meteorological or socioeconomic, so the forecasting model can be improved by considering the interaction amongst the socio-economic activities and environmental concerns. Using granular socioeconomic and meteorological data, deconstructing the mechanism of spillover effects of pollution prevention and a lockdown simultaneously may be another interesting research pursuit.

Author contribution statement

Mingyun Gao: Conceptualization of the presented idea, Software, Validation, Visualization, Writing-Original draft preparation, Formal analysis. Honglin Yang: Supervised the findings of this work. Qinzi Xiao: Data curation, Writing- Original draft preparation. Mark Goh: Writing - Review & Editing, Supervised the findings of this work. All authors discussed the result and contributed to final and revised manuscripts.

Declaration of competing interest

The authors declare that they do not have any competing financial interest nor personal relationships that could have appeared to influence the work reported in this paper.

Acknowledgements

The authors are grateful to the editor and the reviewers for their valuable comments. This work is supported by the China Scholarship Council (CSC) (No. 201906130025, 201906130049), and the National Natural Science Foundation of China (Grant No. 71790593, 72071072).

References

[1] Ocampo L, Yamagishi K. Modeling the lockdown relaxation protocols of the Philippine government in response to the COVID-19 pandemic: an intuitionistic fuzzy DEMATEL analysis. Soc Econ Plann Sci 2020;72:100911. https://doi.org/10.1016/j.seps.2020.100911.
[2] Zhu Y, Chen YQ. On a statistical transmission model in analysis of the early phase of COVID-19 outbreak. Stat. Biosci. 2020. https://doi.org/10.1007/s12561-020-09277-0. online.
[3] Rugani B, Caro D. Impact of COVID-19 outbreak measures of lockdown on the Italian carbon footprint. Sci Total Environ 2020;737:139806. https://doi.org/10.1016/j.scitotenv.2020.139806.
[4] Principato L, Secondi L, Cicatiello C, Mattia G. Caring more about food: the unexpected positive effect of the COVID-19 lockdown on household food management and waste. Soc Econ Plann Sci 2020;74:100953. https://doi.org/10.1016/j.seps.2020.100953.
[5] Wang Q, Han X. Spillover effects of the United States economic slowdown induced by COVID-19 pandemic on energy, economy, and environment in other countries. Environ Res 2021;196:110936. https://doi.org/10.1016/j.envres.2021.110936.
[6] Singh RP, Chauhan A. Impact of lockdown on air quality in India during COVID-19 pandemic. Air Qual Atmos Health 2020;13(8):921–8. https://doi.org/10.1007/s11869-020-00863-1.
[7] Chen K, Wang M, Huang C, Kinney PL, Anastas PT. Air pollution reduction and mortality benefit during the COVID-19 outbreak in China. Lancet Planet Health 2020;4(6):210–2. https://doi.org/10.1016/S2542-5196(20)30107-8.
[8] Sun H, Edziah BK, Sun C, Kporsu AK. Institutional quality and its spatial spillover effects on energy efficiency. Soc Econ Plann Sci 2021;1:101023. https://doi.org/10.1016/j.seps.2021.101023.
[9] Ha-Duong M, Grubb MJ, Hourcade J. Influence of socioeconomic inertia and uncertainty on optimal CO2-emission abatement. Nature 1997;390(6657):270–3. https://doi.org/10.1038/36825.
[10] Lu Y, Li S, Zhong L, Jiang X, Ren F. A clustering-based portfolio strategy incorporating momentum effect and market trend prediction. Chaos, Solit Fractals 2018;117:1–15. https://doi.org/10.1016/j.chaos.2018. 10.012.
[11] Liu L, Wu L. Predicting housing prices in China based on modified Holt's exponential smoothing incorporating whale optimization algorithm. Soc Econ Plann Sci 2020;72:100916. https://doi.org/10.1016/j.seps. 2020.100916.
[12] McCollister GM, Wilson KR. Linear stochastic models for forecasting daily maxima and hourly concentrations of air pollutants. Atmos Environ 1975;9(4):417–23. https://doi.org/10.1016/0004-6981(75)90127-4.
[13] Li J, Tartarini F. Changes in air quality during the COVID-19 lockdown in Singapore and associations with human mobility trends. Aerosol Air Qual Res 2020;20(8):1748–58. https://doi.org/10.4209/aaqr. 2020.06.0303.
[14] Liu Q, Harris JT, Chiu LS, et al. Spatiotemporal impacts of COVID-19 on air pollution in California, USA. Sci Total Environ 2020;750:141592. https://doi.org/10.1016/j.scitotenv.2020.141592.
[15] Liu Q, Malarvizhi AS, Liu W, et al. Spatiotemporal changes in global nitrogen dioxide emission due to COVID-19 mitigation policies. Sci Total Environ 2021;776:146027. https://doi.org/10.1016/j.scitotenv.2021. 146027.
[16] Rodríguez-Urrego D, Rodríguez-Urrego L. Air quality during the COVID-19: PM2.5 analysis in the 50 most polluted capital cities in the world. Environ Pollut 2020;266(1):115042. https://doi.org/10.1016/j.envpol. 2020.115042.
[17] Perera F, Berberian A, Cooley D, et al. Potential health benefits of sustained air quality improvements in New York City: a simulation based on air pollution levels during the COVID-19 shutdown. Environ Res 2021;193:110555. https://doi.org/10.1016/j.envres.2020.110555.
[18] Mullen A, Wang O. China GDP: economy surged record 18.3 per cent in first quarter compared to a year earlier, but slowed versus fourth quarter. South China Morning Post, Accessed 2021-04-16. https://www.scmp. com/economy/china-economy/article/3129758/china-gdp-economy-surged-183-cent-start-2021.
[19] Liu Q, Sha D, Liu W, et al. Spatiotemporal patterns of COVID-19 impact on human activities and environment in mainland China using nighttime light and air quality data. Rem Sens 2020;12(10):1576. https://doi.org/10.3390/rs12101576.
[20] Zhang L, Lin J, Qiu R, et al. Trend analysis and forecast of PM2.5 in Fuzhou, China using the ARIMA model. Ecol Indicat 2018;95(12):702–10. https://doi.org/10.1016/j.ecolind.2018.08.032.
[21] Wang P, Zhang H, Qin Z, Zhang G. A novel hybrid-Garch model based on ARIMA and SVM for PM2.5 concentrations forecasting. Atmos Pollut Res 2017;8(5):850–60. https://doi.org/10.1016/j.apr.2017.01.003.
[22] Lei MT, Monjardino J, Mendes L, Gonçalves D, Ferreira F. Macao air quality forecast using statistical methods. Air Qual Atmos Health 2019;12(9):1049–57. https://doi.org/10.1007/s11869-019-00721-9.
[23] Samal KKR, Babu KS, Das SK, Acharaya A. Time series based air pollution forecasting using SARIMA and Prophet model. In: Proceedings of the 2019 international conference on information Technology and computer communications; 2019. p. 80–5.
[24] Sun W, Sun J. Daily PM2.5 concentration prediction based on principal component analysis and LSSVM optimized by cuckoo search algorithm. J Environ Manag 2017;188:144–52. https://doi.org/10.1016/j.jenvman. 2016.12.011.
[25] García Nieto PJ, Sánchez Lasheras F, García-Gonzalo E, de Cos Juez FJ. PM10 concentration forecasting in the metropolitan area of Oviedo (Northern Spain) using models based on SVM, MLP, VARMA and ARIMA: a case study. Sci Total Environ 2018;621:753–61. https://doi.org/10.1016/j.scitotenv.2017.11.291.
[26] Murillo-Escobar J, Sepulveda-Suescun JP, Correa MA, Orrego-Metaute D. Forecasting concentrations of air pollutants using support vector regression improved with particle swarm optimization: case study in Aburrá Valley, Colombia. Urban Clim 2019;29:100473. https://doi.org/10.1016/j.uclim.2019.100473.
[27] Feng X, Fu T, Cao H, et al. Neural network predictions of pollutant emissions from open burning of crop residues: application to air quality forecasts in southern China. Atmos Environ 2019;204:22–31. https://doi.org/10.1016/j.atmosenv.2019.02.002.
[28] Bai Y, Zeng B, Li C, Zhang J. An ensemble long short-term memory neural network for hourly PM2.5 concentration forecasting. Chemosphere 2019;222:286–94. https://doi.org/10.1016/j.chemosphere.2019.01.121.
[29] Wen C, Liu S, Yao X, et al. A novel spatiotemporal convolutional long short-term neural network for air pollution prediction. Sci Total Environ 2019;654:1091–9. https://doi.org/10.1016/j.scitotenv.2018.11.086.
[30] Bai Y, Li Y, Zeng B, Li C, Zhang J. Hourly PM2.5 concentration forecast using stacked autoencoder model with emphasis on seasonality. J Clean Prod 2019;224:739–50. https://doi.org/10.1016/j.jclepro.2019.03.253.
[31] Zhang B, Zhang H, Zhao G, Lian J. Constructing a PM2.5 concentration prediction model by combining auto-encoder with Bi-LSTM neural networks. Environ Model Software 2020;124:104600. https://doi.org/10.1016/j. envsoft.2019.104600.
[32] Chen L, Pai T. Comparisons of GM (1,1), and BPNN for predicting hourly particulate matter in Dali area of Taichung City, Taiwan. Atmos Pollut Res 2015;6(4):572–80. https://doi.org/10.5094/APR.2015.064.
[33] Xiong P, Yan W, Wang G, Pei L. Grey extended prediction model based on IRLS and its application on smog pollution. Appl Soft Comput 2019;80:797–809. https://doi.org/10.1016/j.asoc.2019.04.035.
[34] Xiong P, Huang S, Peng M, Wu X. Examination and prediction of fog and haze pollution using a Multi-variable Grey Model based on interval number sequences. Appl Math Model 2020;771:531–44. https://doi.org/10.1016/j.apm.2019.09.027.
[35] Wu LF, Li N, Zhao T. Using the seasonal FGM (1, 1) model to predict the air quality indicators in Xingtai and Handan. Environ Sci Pollut Res 2019;26(14):14683–8. https://doi.org/10.1007/s11356-019-04715-z.
[36] Li X, Zhang X. Predicting ground-level PM2.5 concentrations in the Beijing-Tianjin-Hebei region: a hybrid remote sensing and machine learning approach. Environ Pollut 2019;249:735–49. https://doi.org/10.1016/j.envpol. 2019.03.068.
[37] Li Y, Horowitz MA, Liu J, et al. Individual-level fatality prediction of COVID-19 patients using AI methods. Front Public Health 2020;8:587937. https://doi.org/10.3389/fpubh.2020.587937.
[38] Liu Q, Li Y, Yu M, et al. Daytime rainy cloud detection and convective precipitation delineation based on a deep neural network method using GOES-16 ABI images. Remote Sens 2019;11(21):2555. https://doi.org/10.3390/rs11212555.

[39] Dai X, Liu J, Zhang X, Chen W. An artificial neural network model using outdoor environmental parameters and residential building characteristics for predicting the nighttime natural ventilation effect. Build Environ 2019;159:106139. https://doi.org/10.1016/j.buildenv.2019.05.017.
[40] Jin X, Yang N, Wang X, et al. Deep hybrid model based on EMD with classification by frequency characteristics for long-term air quality prediction. Mathematics 2020;8(2):214. https://doi.org/10.3390/math8020214.
[41] Niu M, Gan K, Sun S, Li F. Application of decomposition-ensemble learning paradigm with phase space reconstruction for day-ahead PM2.5 concentration forecasting. J Environ Manag 2017:196110–8. https://doi.org/10.1016/j.jenvman.2017.02.071.
[42] Ventura LMB, de Oliveira Pinto F, Soares LM, Luna AS, Gioda A. Forecast of daily PM 2.5 concentrations applying artificial neural networks and Holt-Winters models. Air Qual Atmos Health 2019;12(3):317–25. https://doi.org/10.1007/s11869-018-00660-x.
[43] Pai T, Hanaki K, Chiou R. Forecasting hourly roadside particulate matter in Taipei county of Taiwan based on first-order and one-variable grey model. Clean 2013;41(8):737–42. https://doi.org/10.1002/clen.201000402.
[44] Zhang Z, Wu L, Chen Y. Forecasting PM2.5 and PM10 concentrations using GMCN (1, N) model with the similar meteorological condition: case of Shijiazhuang in China. Ecol Indicat 2020;119:106871. https://doi.org/10.1016/j.ecolind.2020.106871.
[45] Xiao Q, Gao M, Xiao X, Goh M. A novel grey Riccati-Bernoulli model and its application for the clean energy consumption prediction. Eng Appl Artif Intell 2020;95:103863. https://doi.org/10.1016/j.engappai. 2020.103863.
[46] Xiao Q, Shan M, Gao M, Xiao X, Guo H. Evaluation of the coordination between China's technology and economy using a grey multivariate coupling model. Technol Econ Dev Econ 2021;27(1):24–44. https://doi.org/10.3846/tede.2020.13742.
[47] Xiang X, Ma X, Ma M, Wu W, Yu L. Research and application of novel Euler polynomial-driven grey model for short-term PM10 forecasting. Grey Syst 2020. https://doi.org/10.1108/GS-02-2020-0023. online.
[48] Zhao G, Huang G, He H, Wang Q. Innovative spatial-temporal network modeling and analysis method of air quality. IEEE Access 2019;726:241–54. https://doi.org/10.1109/access.2019.2900997.
[49] Cheng Z, Li L, Liu J. Identifying the spatial effects and driving factors of urban PM2.5 pollution in China. Ecol Indicat 2017;82:61–75. https://doi.org/10.1016/j.ecolind.2017.06.043.
[50] Li L, Wu AH, Cheng I, Chen J, Wu J. Spatiotemporal estimation of historical PM2.5 concentrations using PM10, meteorological variables, and spatial effect. Atmos Environ 2017;166:182–91. https://doi.org/10.1016/j. atmosenv.2017.07.023.
[51] Yang C, Sha D, Liu Q, et al. Taking the pulse of COVID-19: a spatiotemporal perspective. Int J Digit Earth 2020;13(10):1186–211. https://doi.org/10.1080/17538947.2020.1809723.
[52] Liu Q, Liu W, Sha D, et al. An environmental data collection for COVID-19 pandemic research. Data 2020;5(3):58. https://doi.org/10.3390/data5030068.
[53] Miri M, Ghassoun Y, Dovlatabadi A, Ebrahimnejad A, Löwner M. Estimate annual and seasonal PM1, PM2.5 and PM10 concentrations using land use regression model. Ecotoxicol Environ Saf 2019;174:137–45. https://doi.org/10.1016/j.ecoenv.2019.02.070.
[54] Xu X, Zhang T. Spatial-temporal variability of PM2.5 air quality in Beijing, China during 2013-2018. J Environ Manag 2020;262:110263. https://doi.org/10.1016/j.jenvman.2020.110263.
[55] Bigi A, Ghermandi G. Trends and variability of atmospheric PM2.5 and PM10-2.5 concentration in the Po Valley, Italy. Atmos Chem Phys 2016;16(24):15777–88. https://doi.org/10.5194/acp-16-15777-2016.
[56] Singh V, Singh S, Biswal A. Exceedances and trends of particulate matter (PM2.5) in five Indian megacities. Sci Total Environ 2020;750:141461. https://doi.org/10.1016/j.scitotenv.2020.141461.
[57] Cleveland RB, Cleveland WS, McRae JE, Terpenning I. STL: a seasonal-trend decomposition. J Off Stat 1990;6(1):3–73.
[58] Feng X, Wang S. Influence of different weather events on concentrations of particulate matter with different sizes in Lanzhou, China. J Environ Sci-China 2012;24(4):665–74. https://doi.org/10.1016/S1001-0742(11)60807-3.
[59] Huang C, Shen Y, Kuo P, Chen Y. Novel spatiotemporal feature extraction parallel deep neural network for forecasting confirmed cases of coronavirus disease. Soc Econ Plann Sci 2019:2020100976. https://doi.org/10.1016/j.seps.2020.100976.
[60] Xiao Q, Shan M, Gao M, Xiao X, Goh M. Parameter optimization for nonlinear grey Bernoulli model on biomass energy consumption prediction. Appl Soft Comput 2020;95:106538. https://doi.org/10.1016/j.asoc. 2020.106538.
[61] Anselin L. A note on small sample properties of estimators in a first-order spatial autoregressive model. Environ Plann A 1982;14(8):1023–30. https://doi.org/10.1068/a141023.
[62] Mao S, Kang Y, Zhang Y, Xiao X, Zhu H. Fractional grey model based on non-singular exponential kernel and its application in the prediction of electronic waste precious metal content. Isa T 2020:10712–26. https://doi.org/10.1016/j.isatra.2020.07.023.
[63] Gao M, Yang H, Xiao Q, Goh M. A novel fractional grey Riccati model for carbon emission prediction. J Clean Prod 2021;282:124471. https://doi.org/10.1016/j.jclepro.2020.124471.
[64] Mao S, Zhu M, Wang X, Xiao X. Grey Lotka-Volterra model for the competition and cooperation between third-party online payment systems and online banking in China. Appl Soft Comput 2020;95:106501. https://doi.org/10.1016/j.asoc.2020.106501.
[65] Xiao X, Duan H. A new grey model for traffic flow mechanics. Eng Appl Artif Intell 2020;88:103350. https://doi.org/10.1016/j.engappai.2019.103350.
[66] Ma J, Ding Y, Cheng JC, Jiang F, Wan Z. A temporal-spatial interpolation and extrapolation method based on geographic long short-term memory neural network for PM2.5. J Clean Prod 2019;237:117729. https://doi.org/10.1016/j.jclepro.2019.117729.
[67] Qing X, Niu Y. Hourly day-ahead solar irradiance prediction using weather forecasts by LSTM. Energy 2018:148461–8. https://doi.org/10.1016/j.energy.2018.01.177.
[68] LeSage JP, editor. The theory and practice of spatial econometrics. Toledo: University of Toledo; 1999. p. 12.[69] Dai J, Liu H, Sun Y, Wang M. An optimization method of multi-variable MGM(1,m) prediction model's background value. J Grey Syst 2018;30(1):221–39.
[70] Zhang G, Lu H, Dong J, et al. A framework to predict high-resolution spatiotemporal PM2.5 distributions using a deep-learning model: a case study of Shijiazhuang, China. Remote Sens 2020;12(17):2825. https://doi.org/10.3390/rs12172825.
[71] Zheng H, Kong S, Chen N, et al. Significant changes in the chemical compositions and sources of PM2.5 in Wuhan since the city lockdown as COVID-19. Sci Total Environ 2020;739:140000. https://doi.org/10.1016/j. scitotenv.2020.140000.
[72] Li Q, Guan X, Wu P, et al. Early transmission dynamics in Wuhan, China, of novel Coronavirus–infected pneumonia. N Engl J Med 2020;382(13):1199–207. https://doi.org/10.1056/NEJMoa2001316.
[73] Wang Y, Yuan Y, Wang Q, et al. Changes in air quality related to the control of coronavirus in China: implications for traffic and industrial emissions. Sci Total Environ 2020;731:139133. https://doi.org/10.1016/j.scitotenv.2020.139133.
[74] Lu Q, Cai Z, Chen B, Liu T. Social policy responses to the covid-19 crisis in China in 2020. Int J Environ Res Publ Health 2020;17(16):5896. https://doi.org/10.3390/ijerph17165896.
[75] Tønnessen Ø, Dhir A, Flåten BT. Digital knowledge sharing and creative performance: work from home during the COVID-19 pandemic. Technol Forecast Soc 2021;170:120866. https://doi.org/10.1016/j.techfore. 2021.120866.
[76] Zhang H, Song H, Wen L, et al. Forecasting tourism recovery amid COVID-19. Ann Tourism Res 2021;87:103149. https://doi.org/10.1016/j.annals.2021.103149.
[77] Deng JL. Introduction to grey mathematical resource science. first ed. Wuhan: Huazhong University of Science and Technology Press; 2010.

Mingyun GAO was born in 1990. He is a Ph.D. student from Management Science and Engineering in School of Business Administration at Hunan University, China. Gao received B.S. and M.S. degrees from Wuhan University of Technology, China. His research interests are operations research and management sciences, grey forecasting theory, supply chain finance and logistics optimization. E-mail: wh14_gao@126.com

Honglin YANG is a professor of School of Business Administration at Hunan University, China. He earned his Ph.D. in Management Science and Engineering from Hunan University China. His research interests include operating system optimization, industrial economy and technical economic evaluation, supply chain finance, intelligent supply chain innovation and management. E-mail: ottoyang@126.com; ottoyang@hnu.edu.cn

Qinzi XIAO was born in 1991. She is a Ph.D. student from Management Science and Engineering in School of Business Administration at Hunan University, China. Xiao received M.S. degrees from University of Birmingham, UK. Her research interests are operating system optimization, quality management. E-mail: qzxiao97@hnu.edu.cn

Mark GOH is currently a Professor in the NUS Business School & The Logistics Institute-Asia Pacific at National University of Singapore. He earned a Ph.D. from the University of Adelaide. His current research interests are supply chain management, purchasing, quality and healthcare, service operations. E-mail: mark_goh@nus.edu.sg; bizgohkh@nus.edu.sg